

AD-A216 540

5528-MS-01 (2)

**SPALLATION AND DYNAMIC FRACTURE
AS AN EFFECT OF LASER INDUCED
SHOCK WAVES IN CARBON BASED
COMPOSITE MATERIALS**

Principal Investigators: Dr. S. Eliezer and Dr. I. Gilath
October 1989

Final Technical Report

DTIC
ELECT
JAN 08 1990
S B D

United States Army
European Research Office of the U.S. Army
London, England

Contract Number: DAJA45-87-C-0032

Approved for Public Release ; distribution unlimited.

Plasma Physics Department

SOREQ N.R.C.

Yavne 70600

ISRAEL

90 C1 0.5

Unclassified

SECURITY CLASSIFICATION OF THIS PAGE (When Data Entered)

REPORT DOCUMENTATION PAGE		READ INSTRUCTIONS BEFORE COMPLETING FORM
1. REPORT NUMBER	2. GOVT ACCESSION NO.	3. RECIPIENT'S CATALOG NUMBER
4. TITLE (and Subtitle) SPALLATION AND DYNAMIC FRACTURE AS AN EFFECT OF LASER INDUCED SHOCK WAVES IN CARBON BASED COMPOSITE MATERIALS		5. TYPE OF REPORT & PERIOD COVERED Final Report
3. AUTHOR(s) S. Eliezer, I. Gilath		6. PERFORMING ORG. REPORT NUMBER
9. PERFORMING ORGANIZATION NAME AND ADDRESS Soreq Nuclear Research Centre Yavne , 70600, ISRAEL		8. CONTRACT OR GRANT NUMBER(s) DAJA45 - 87 - C - 0032
11. CONTROLLING OFFICE NAME AND ADDRESS U.S. Army Research, Development and Standardization Group, 223 Old Marylebone Rd, London NW1 5TH, UK		10. PROGRAM ELEMENT, PROJECT, TASK AREA & WORK UNIT NUMBERS
14. MONITORING AGENCY NAME & ADDRESS (if different from Controlling Office)		12. REPORT DATE October 1989
		13. NUMBER OF PAGES 43
		15. SECURITY CLASS. (of this report) Unclassified
16. DISTRIBUTION STATEMENT (of this Report)		15a. DECLASSIFICATION/DOWNGRADING SCHEDULE
17. DISTRIBUTION STATEMENT (of the abstract entered in Block 20, if different from Report)		
18. SUPPLEMENTARY NOTES		
19. KEY WORDS (Continue on reverse side if necessary and identify by block number) Spallation, Fracture, Composite Materials, laser induced shock wave attenuation, ultra high strain rate phenomena		
20. ABSTRACT (Continue on reverse side if necessary and identify by block number) A high irradiance single beam short pulsed Nd:glass laser was used to generate shock waves in carbon-carbon and carbon epoxy composites. Dynamic brittle fracture at hypervelocity impact conditions was observed as a result of reflected shock waves as tensile waves from the back surface of samples. Successive stages of damage from incipient spallation to complete sample perforation were obtained by increasing gradually the laser energy. The		

DD FORM 1473 1 JAN 73 EDITION OF 1 NOV 68 IS OBSOLETE

Unclassified
SECURITY CLASSIFICATION OF THIS PAGE (When Data Entered)

thermo-mechanical damage on the front surface as a result of laser interaction with the target material, and the mechanical damage at the back surface as a result of shock wave reflection were characterized by optical and scanning electron microscopy. The failure properties of the carbon composites were related to the processing of densification and graphitization mode. While the failure properties for carbon epoxy composites were related to impact direction versus fiber direction. A comparison was made between spall properties of carbon epoxy composites with aluminum and iron.

A new experimental method was developed to calculate the attenuation of laser generated shock waves. This technique enables also the evaluation of the laser induced spall pressure in different materials.

Accession For	
NTIS GRA&I	<input checked="" type="checkbox"/>
DTIC TAB	<input type="checkbox"/>
Unannounced	<input type="checkbox"/>
Justification	
By	
Distribution/	
Availability Codes	
Dist	Avail and/or Special
A-1	

**SPALLATION AND DYNAMIC FRACTURE AS AN EFFECT OF LASER INDUCED SHOCK WAVES IN
CARBON BASED COMPOSITE MATERIALS.**

TABLE OF CONTENTS

1. INTRODUCTION

- 1.1 Objectives
- 1.2 Laser induced shock waves
- 1.3 Estimation of the strain rate
- 1.4 Experimental method

2. DAMAGE IN CARBON-CARBON COMPOSITES

- 2.1 Introduction
- 2.2 Composite preparation
- 2.3 Experiments and results
- 2.4 Conclusion

**3. DAMAGE IN CARBON EPOXY UNIDIRECTIONAL COMPOSITES AS COMPARED TO
ALUMINUM AND IRON**

- 3.1 Introduction
- 3.2 Composite preparation
- 3.3 Experimental
- 3.4 Laser impact perpendicular to the fiber direction
- 3.5 Laser impact parallel to the fiber direction
- 3.6 Conclusion

4. EXPERIMENTAL ESTIMATION OF THE SHOCK WAVE ATTENUATION

- 4.1 Introduction
- 4.2 Experimental results

5. DISCUSSION

REFERENCES

TABLES

FIGURE CAPTIONS

1. INTRODUCTION

1.1 Objectives

Shock loads can be generated by high speed impact, explosives or by intense short time energy deposition. While in most impact experiments the impact time is in the microsecond time scale, the laser impact time is in the nanosecond regime.

There is a considerable interest in determining the response of composite materials to shock loads since they are increasingly being used in applications where shock loading is significant. It is important to know the stages of material failure, in particular the conditions of incipient damage and the pressure responsible for this damage as well as the pressure attenuation in the sample.

Some composites such as carbon-carbon are used for components which should withstand high temperatures as well as impacts. Carbon-epoxy composites are replacing high performance metal parts in space components due to their high strength to weight ratio. The compressive and tensile strength of carbon based composites is seriously reduced by impact damage¹⁻⁴. These materials were also tested for their thermal response to characterize the effect of heat blast⁵. Experimental work has been performed to establish the ablative characteristics of some composites using continuous wave CO₂ laser⁶⁻⁸. There is however no published work on the impact behaviour of composites using short pulsed laser induced impact. To our knowledge we are the first to investigate this subject.

Our work is based on our previous experience on spall and dynamic fracture in metals⁹⁻¹³. The advantage of our method as compared to other impact experiments is the study of thermomechanical damage at strain rates of the order of 10^7 sec^{-1} , corresponding to hypervelocity impact conditions. Other advantages are the small quantity of material involved and the close control of experimental conditions. Basically we can observe the following failure modes for composites as a result of laser induced shock waves: ablation damage (at the impact site), matrix cracking, fiber-matrix debonding, fiber breakage, back surface spallation and complete perforation.

We believe that our data will contribute to the understanding of the thermomechanical damage development in composites of interest at hypervelocity impact conditions. The objective of this work is to gain insight into the fracture behaviour of composites at ultra high strain rate under tensile impact loading.

1.2 Laser induced shock waves

The interaction physics between high irradiance lasers ($\approx 10^{10} \text{ W/cm}^2$) and matter, leading to the creation of a shock wave, can be summarized schematically by the following intercorrelated processes:

LASER ABSORPTION → ENERGY TRANSPORT → SHOCK WAVE

The irradiated target creates a plasma (corona) instantaneously ($< 10^{-12} \text{ sec}$), so that during the laser pulse duration (of the order of nanoseconds in our case) the irradiated matter consists of a plasma medium in front of the dense target (solid density). The laser radiation entering the plasma encounters increasing density of plasma and it is absorbed up to the critical density region where the plasma frequency equals that of the laser light. The plasma refractive index becomes zero at the critical density (where the resonant frequency of the plasma electrons in the oscillating electric field is equal to the laser frequency) so that

reflection of the laser light occurs in this region. The critical density n_c is given by

$$n_c = 10^{21}/\lambda^2 \text{ electrons cm}^{-3}$$

where the laser wavelength λ is given in microns. (Our laser wavelength is about 1 micron). For a fully ionized plasma (where the atomic mass $A \sim 22$) the critical density corresponds to a mass density of

$$\rho_c = 3.3 \times 10^{-3} \lambda^{-2} \text{ g/cm}^3$$

so that in general the critical mass density is small relative to solid density. In our regime of irradiance ($10^{10} - 10^{12} \text{ W/cm}^2$) the laser absorption is through the inverse bremsstrahlung mechanism in which an electron in binary collision with an ion absorbs a photon.

The energy is carried away from the point of absorption by the diffusion process. The energy absorbed by the electrons up to the critical density is transported outward into the expanding plasma and inwards into the plasma of greater than critical density. The inward transport of energy reaches the ablation surface where the plasma is created.

In laser-matter interaction under consideration the inward momentum is imparted to the target by the ablation of the hot plasma rather than by the momentum of the laser photon themselves. The heated material is blown off the target and the ablation drives a shock wave into the target. At the final stages of the laser pulse the ablation pressure at the surface drops and a rarefaction wave propagates into the target, following the shock wave. This pressure wave is approximately of a triangular shape and it propagates into the target. After reaching the back surface of the target it is reflected and a tension (negative pressure) is created. In fig 1.1, a schematic representation of the creation of a negative pressure pulse can be seen. For a triangular pressure pulse with a maximum pressure P_0 reaching the free surface of the target, a spall is formed at a distance Δ , by the spall pressure $-P_s$ (the negative pressure required for spall.) There is a minimum value, $P_0 = P_s$, for spall to occur. For higher values of P_0 , multiple spall layers can be obtained in brittle materials while for ductile material the energy is dissipated in plastic deformation.

The values of ablation induced shock pressure can be calculated by sophisticated hydrodynamic simulation codes. However, to a good approximation for our laser irradiances an analytic quantitative estimate of the ablation pressure is given by the following formula¹⁴.

$$P_{kb} = 230 A^{7/6} z^{-9/16} \lambda^{-1/4} \tau^{-1/8} \left[\frac{I}{10^{12}} \right]^{3/4} \quad (1.1)$$

where, the pressure is given in kilobars, A is the atomic weight, z the ionization number, λ the laser wavelength in μm , τ the laser pulse time in nanoseconds and I is the laser intensity in W/cm^2 .

Using our laser induced shock waves, spall in metallic targets was investigated by us and all stages of damage or dynamic failure were identified⁹⁻¹³. The intensities of the 3.5 nsec Nd:Glass laser were in the range of $10^{10} - 10^{12} \text{ W/cm}^2$, and the foil thickness was in the 100-600 μm range. The laser-generated shock wave pressure was in the range of a few hundred kilobars (kb). The shock wave traversed the foils in a few tens of

nsec. The controlled stepwise increase in laser energies allowed us to find the stages of damage evolution from incipient to complete perforation of the target foils. The incipient spall for ductile metals was identified from the level of separate voids in aluminium, while brittle metals from the level of cracks. Those voids or cracks coalesce resulting in a continuous spall layer. For higher laser intensities the spall layer break away and target penetration is observed for specific high intensities. In this report the dynamic fracture of carbon based composites is investigated.

1.3 Estimation of the strain rate

Strain rate estimates were done for aluminium using experimental and simulation results.

The strain rate in ballistic experiments is estimated¹⁵ as $\dot{\epsilon} = \Delta\epsilon/\Delta t$, where $\Delta\epsilon = 2U_p/C$, where U_p is the particle velocity and C is the speed of sound. This gives only a very rough estimate of the strain rate, as Grady¹⁵ himself comments: "Variations in strain rate among experiments are a consequence of differing amounts of dispersion before wave interaction at the spall plane". The exact strain rate associated with spall for impact times of a few nanoseconds is difficult to determine accurately. Using the analogy of laser experiments for strain rate calculations, Δt , can be substituted by τ_L the laser pulse time. The strain for laser experiments can be written in the same way, and the rough estimate for the strain rate is accordingly:

$$\dot{\epsilon} = \frac{2 U_p}{C \tau_L} \text{ sec}^{-1} \quad (1.2)$$

By substituting values from equation of state for aluminum in our experimental range of a few hundred kb, we obtain the following strain rate

$$\dot{\epsilon} = (3-4) \times 10^7 \text{ sec}^{-1}$$

The computer simulation of the phenomena of laser-solid interactions and the material behaviour involves the simultaneous solution of the three conservation equations (of mass, momentum and energy), along with the equation of state (EOS) of the material. As long as the size of the laser spot is larger by a factor of 3 than the foil thickness, one can employ a one dimensional computer code. In our simulation¹³ we use a simple spall model in which the material is spalled at the cell whose (negative) pressure attains a value more negative than the 'spall pressure'.

The strain rate can be calculated from the simulation as following:

$$\dot{\epsilon} = \frac{-\dot{\rho}}{\rho} = -\frac{1}{\rho} \frac{\partial \rho}{\partial t} = -\frac{1}{\rho} \frac{\partial \rho}{\partial x} C \quad (1.3)$$

where $\partial \rho / \partial x$ is the density gradient obtained from the simulations at time and position right before the spall occurs, and C is the speed of sound. The density gradient is laser intensity dependent. In our simulations for

aluminium in the domain of laser irradiance $10^{10} - 10^{12}$ W/cm² the density gradient varies in the range of -5×10^6 to -2×10^7 kg/m⁴. Therefore the strain rate will be in the range of $(1-4) \times 10^7$ sec⁻¹, in agreement with the strain rate calculated above.

The strain rates we obtained are about one order of magnitude larger than those obtained by the other experimental methods

1.4 The experimental method

The Advanced Laser Amplifier Design Integration System is capable of delivering 3-10 nsec, up to 100 Joule pulses in the 1.06 μ m wavelength (see Fig. 1.2). The system comprises three stages: the pulse forming and pre-amplifying stage, the filtering stage and the main amplifying stage.

The first stage contains a Q-switched oscillator which delivers Gaussian shaped pulses with variable FWHM between 3-10 nsec. This Gaussian shape can be modified by steepening its edges for shock wave production by using a fast electro-optical shutter.

The second stage includes spatial filters (SF) defining the appropriate divergence needed for the third stage. Optical isolation is also included to avoid back reflection of the amplified beam.

The third stage includes a triple pass amplifier (7³) with its associated optics and a double pass amplifier (8²)

The amplified beam is focused in the target chamber (TC) through a f/20 lens. For our experiments the beam intensity obtained is in the range $10^{10} - 10^{12}$ W/cm². For spall experiments, where lower intensities and larger spots are required, 1-3 mm diameter spots can be obtained by moving the target (T) out of focus.

The diagnostics include routine monitoring of beam characteristics, such as energy, temporal and spatial shape, by means of a calorimeter, optical streak camera, various X-ray diagnostics etc. The laser system is described in more detail in ref 17

Fig 3 is a partial view of the amplifier stage and fig 4 is the target chamber

The experimental work consisted of determining the irradiance and energy density conditions required to produce spall in one dimensional shock wave geometry.

Very close energy density steps can be obtained at the amplifier stages, enabling to monitor all failure stages.

For damage evaluation, metallurgical or scanning electron microscopy was used. For internal damage evaluation, the samples were sectioned, polished, and examined by optical microscopy.

2. DAMAGE IN 2D CARBON-CARBON COMPOSITES

2.1 Introduction

Carbon-carbon (C/C) composites are a relatively new class materials that provide superior thermal and mechanical properties for temperatures above 2000°C, that no other material can provide.

The C/C composites family is characterized by a carbonaceous matrix, reinforced with carbon or graphite fibers having a two-or multidimensional resin-fiber system¹⁹. The matrix also contributes to the mechanical properties of the composites.

The effect of condensation of carbon vapor and hardening of the surface in the region of burned spots as a results of pulsed laser radiation of moderate power (3.7×10^5 W/cm²) was studied by Loshkarav⁷. The ablation properties of carbon-carbon composites were studied by Evangelides⁸ using a CO₂ laser.

In this chapter we report, various stages in composite failure which were obtained by pulsed high irradiance laser induced shock waves. The dynamic failure properties and spallation of the composites are related to their densification mode.

2.2 Composite preparation

Bidirectionally reinforced (2D) carbon-carbon composites were prepared from Hexcel 4C1008, 8 Harness, satin weaving carbon fabric reinforcement (Hexcel, California) by carbonization, graphitization and densification.

Hexel 4C 1008 consists of a carbonaceous filler, a high temperature phenolic resin binder, reinforced with carbon fabric. The reinforcement content is 58%, while the filler content 8% and the phenolic resin content is 34%. After curing at 160°C and 1000 psi the material was carbonized at 1000°C, at atmospheric pressure in inert gas flow. The overall processing time of slow heating and cooling rates were 62 hours. The final phenolic char residue after carbonization has a volume fraction of 0.13. This material is defined as "original" and is denoted by "O" in Table 2.1

The graphitization (G) is performed at 2600°C for 8 hours at atmospheric pressure in an inert gas. The degree of graphitization was measured through crystalline parameters using X-ray diffraction. The degree of graphitization was exceeding 50% for every cycle.

The phenolic char is partially transformed in glassy carbon during the carbonization which is not crystallized by graphitization. The glassy carbon was observed by scanning electron microscopy.

The densification was performed by impregnation with coal-tar pitch. Two densification methods were used

- (a) One densification cycle by pitch impregnation at low pressure and carbonization in a Hot-Isostatic Press (H) at 1000 atm, and 650°C. This material is denoted by 1(H + G) in Table 2.1.
- (b) Four densification cycles at atmospheric pressure (A) by dipping in molten pitch and carbonization in inert atmosphere at normal pressure and 1000°C. This material is denoted 4(A + G) in Table 2.1. Densities obtained by the two methods were almost identical.

Sample thicknesses for laser experiments were reduced to 0.55 mm by diamond saw cutting and polishing. The direction of cutting is parallel to 2D reinforcement, as can be seen also by the scanning electron micrographs.

The two-dimensional (2D) samples used to compare their structural properties to thermo-mechanical damage by pulsed laser induced shock waves are summarized in Table 2.1

2.3 Experiment and results

A high irradiance single beam pulsed Nd:glass laser was used to generate the shock waves in the C/C composite. In our experiments we use a modified Gaussian laser pulse with 3.5 nsec full width at half maximum intensity level (FWHM). The sensitivity of our results to the laser pulse duration were checked by repeating some of the experiments with a pulse time duration of 7.5 nsec.

Different energy levels were applied to determine stages of material failure from incipient to total perforation (burn through) of the sample, by a similar procedure used by us to study spallation and dynamic fracture in metals at ultra high strain rate⁹⁻¹³.

Scanning electron microscopy was used to evaluate some characteristic damage stages.

Successive stages of damage in carbon-carbon composites were obtained by gradually increasing the laser energy. Brittle failure mode was observed for all samples. The strain of these fibers is generally very small and can be considered to be within the elastic limits.

The reflected shock wave pressure from the back surface of the sample is responsible for spallation and is indicative of the tensile failure. The shock pressure is scaling with the laser irradiance. The irradiance values for threshold back surface spallation are summarized in Table 2.2.

The tensile failure as a result of laser induced shock waves of the densified samples 4(A + G) and 1(H + G) are practically similar but higher than the O + G sample.

Sample perforation is scaling with energy density. As it can be seen from Table 2.3 there are considerable differences in perforation energy density as a result of densification and densification mode.

No penetration (burn through) was obtained for sample 1(H + G) for the range of energy densities used.

The above experiments were done for two pulse lengths: 3 and 7.5 nsec FWHM. The back surface damage depends on the laser irradiance while perforation were practically a function of the energy density.

Comparing Tables 2.2 and 2.3, large differences can be seen between threshold energies for back surface spallation and energies for perforation.

The following scanning electron micrographs are illustrating different stages of failure, as observed during the experiments.

Successive stages of damage are presented for 4(A + G) samples in Figures 2.1-2.5 corresponding to incipient back surface damage to complete perforation. In fig. 2.6 front surface perforation corresponding to back surface (see fig. 2.5) is presented. An example of fractured glassy carbon can be seen in fig. 2.7. Front surface (laser side) damage of the 1(H + G) were far lower as compared to samples 4(A + G) or O + G. In fig. 2.8 only a slight damage can be seen on the front side of 1(H + G) sample at 5.9 kJ/cm², while for the same energy density a 4(A + G) sample was already perforated. At higher magnification, some interesting details were observed on the front side for irradiances exceeding 10¹² Watt/cm² (see figures 2.9-2.10). These irradiances correspond to temperatures about 10⁵K and pressures about 250 kilobars on the ablation surface. The plasma temperature and the induced ablation pressure is calculated by using a simple analytical model (see chapter 1). For carbon (or other elements) a laser-plasma simulation¹⁶ was used in order to estimate temperature and pressures on the target side which interacts with the laser. In fig. 2.9 there is evidence of resolidified molten fibers in a very rapid process. In fig. 2.10 an amorphous fluffy phase is presented which it seems originated

from the very rapid heating of the matrix. These features have been observed only in the densified (impregnated) samples above irradiances of 10^{12} watt/cm².

2.4 Conclusion

Experiments were performed to compare the impact resistance of carbon-carbon composites to short pulsed laser induced shock waves²⁰. Densification by hot isostatic press provided a better perforation resistance material as compared to material densified at atmospheric pressure. The dynamic tensile strengths for 4(A + G) and 1(H + G) are comparable. Their strengths are larger by about a factor of 3 than that of (O + G).

The above experiments analysed planar shock waves for two pulse length: 3 and 7.5 nsec. The threshold back surface damage depends on the laser irradiance (W/cm²) while the perforation phenomenon is a function of the energy density (J/cm²).

3. DAMAGE IN CARBON EPOXY UNIDIRECTIONAL COMPOSITE AS COMPARED TO ALUMINUM AND IRON

3.1 Introduction

A continuous replacement of conventional metals by composite materials is observed in space applications. It is due to their superior mechanical properties, high strength to low weight ratio and high chemical resistivity.

Carbon fibers (CF) are among the most promising reinforcing materials for composites having very high modulus and strength, high stiffness, low density, low coefficient of thermal expansion, good fatigue and creep resistance, dimensional stability and transparency to X-rays. Carbon fibers are chemically inert, show good resistance to stress corrosion and other environmental degradation.

In the present work, the impact properties at ultra high strain rate ($\dot{\epsilon} \sim 10^7 \text{ s}^{-1}$) will be studied, using short pulsed laser induced shock waves.

A comparison will be made between the impact behaviour at ultra high strain rate of CF/epoxy, aluminum and iron in order to evaluate their relative strength for short pulsed laser induced shock waves.

Two impact directions will be used for CF/epoxy composite: parallel and perpendicular to fiber directions.

The resistances of CF/epoxy composites, aluminum and iron were also evaluated by the Charpy method, according to ASTM D 256.

3.2 Preparation of the composite specimens

The unidirectional composite specimens were prepared from CF obtained from ACF kibbutz Afikim, Israel.

The ACIF-XHT coding system of the fibers refers to extra high strength CF manufactured from polyacrylonitrile with tows containing 6000 filaments. The diameter of a single filament is 7 μm . Typical properties are presented in table 3.1.

The composites were prepared in a rectangular mold spread with a very thin layer of wax to avoid glueing of the epoxy matrix. The filament tows were soaked with epoxy and stretched along the axis of the mold. The epoxy was prepared by mixing preheated Tonox 60/40 and DER-330, with RD-2 as diluter at 60°C. Between each addition of new layers of tows, the inner part of the mold was saturated with epoxy. These steps were continued until the desired amount of CF was put in the mold. The plunger was mechanically pressed into the inner part of the mold. The pressed mold was subjected to two curing steps: 3 h at 80°C and one h at 140°C. The mold was cooled to room temperature and then unassembled. The fiber content of the composites was $60 \pm 2\%$. Several composite sample thicknesses were prepared from 0.2 to 2 mm.

The aluminum and iron foils were purchased from Goodfellow (England). Aluminum foil thicknesses were 0.1, 0.175, 0.275, and 0.6 mm. Iron foils were 0.1 and 0.25 mm thickness. Typical properties are presented in Table 3.1.

3.3 Impact experiments

The high strain rate impact experiments were performed with the Nd:glass laser. The pulse length was 7.5×10^{-9} sec and irradiances of the

order of 10^{10} - 10^{11} Watt/cm² were used to obtain threshold for spall in samples of different thicknesses.

Laser energies were changed stepwise to ensure damage evolution measurements. Laser spots were three times greater than sample thicknesses to ensure planar shock waves.

Scanning electron microscopy was performed on a JEOL ISM-1300 instrument at 25 KV on gold coated samples.

Mechanical sectioning and polishing was used to reveal internal damage.

The low strain rate impact experiments of the CF/epoxy composite, aluminum and iron were evaluated by the Charpy method. This test uses a pendulum type hammer where the energy to break the sample is measured by one pendulum swing. The dimensions of the specimens were 50 x 10 x 2 mm. A notch was made in the middle of the specimen on the shorter side. The depth of the notch was 20% of the width of the sample. The notch was made using a milling cutter (Schmidt, model K-20) and the profile was checked in a comparator (Mitutoyo, model PJ 311). The impact tests were performed on a standard instrument (Zwick type S101, 50 joules maximum energy capacity). The average result for 9 samples is reported in table 3.2.

3.4 Impact experiments perpendicular to the fiber direction

The laser energy was applied perpendicular to the fiber direction of the composites. The spall damage was observed as fiber and matrix breaking at the back surface of the samples, the damage increasing with increasing laser energy densities²⁷. The threshold energy density and corresponding irradiances and plasma ablation pressure to produce spall in composites, aluminum and iron are presented in table 3.3. Plasma ablation pressure was calculated using eq. 1 of chapter 1.

In fig. 3.1, laser threshold energies are shown for different target thicknesses for CF/epoxy, aluminum and iron. An additional data for 2D carbon/carbon composite²⁰ is presented for comparison. Damage development for different composite thicknesses is similar. Some typical damage stages for damage development are presented for a 0.5 mm sample thicknesses, see figures 3.2 - 3.10.

Figure 3.2 represents front surface damage in carbon epoxy composites. It can be seen that the damage consists mainly of a shallow crater due to epoxy ablation and breaking of a few fibers. In fig. 3.3, a detail from fig. 3.2 is shown. Only the clean fibers are seen as a result of epoxy ablation. The mild damage on the front (laser side) correspond to severe spall damage on the back side, see following figures (3.5-3.9).

In fig. 3.4, a detail is shown from a front crater in aluminum. Due to its low melting point, craters are easily formed and some of the molten aluminum is splashed around the lips of the crater.

Figures 3.5-3.9 show a sequence of damage development at the back free surface of the samples as a result of reflected shock waves. It is interesting to remark that incipient damage occurs at a relatively low energy density (195 J/cm^2 for a 0.5 mm sample), however, penetration of the sample was not achieved at 1500 J/cm^2 for one dimension shock wave condition (laser spot diameter of 2 mm for a 0.1 mm sample thickness). Also penetration of the carbon epoxy sample was not obtained for a focused beam of 50 KJ/cm^2 .

In fig. 3.8 a detail is shown from back surface damage. Some of the matrix is still attached to the fiber as compared to front surface damage fig. 3.3 where the matrix is completely ablated.

Figure 3.10 represents a cross section through a 2 mm sample. No internal delamination was observed for the sectioned samples.

Incipient spall in aluminum is shown in figure 3.11 and for iron in fig. 3.12. No internal damage such as cracks or delaminations were found in CF/epoxy samples when laser impact was perpendicular to fiber direction.

3.5 Impact experiments parallel to the fiber direction.

Impact experiments parallel (along the fiber direction) revealed a greater resistance than in the perpendicular direction, as expected. The undamaged material can be seen in fig. 3.13 and after impacting in fig. 3.14.

Front laser side surface damage is characterized by radial or irregular cracking see fig. 3.15 and 3.16. Cracks may extend far away from the impact site due to matrix cracking. A detail from the front (impact site can be seen in fig. 3.17); the picture was taken with a tilt angle of 60° for better observation. The smooth appearance of the bare carbon fibers without matrix is a result of the local heating during ablation. The matrix was ablated to a depth of a few microns up to a maximum of 20 µm.

Fig. 3.18 is representing the area of the periphery of the impact site. Some of the fibers are bare and the epoxy is lifted due to excessive heat.

Back surface cracking can be seen in fig. 3.19. Fig. 3.20 is a detail from back surface damage showing fiber and matrix breaking, quite different from front surface damage. A typical fiber breaking is well seen in fig. 3.21 as compared to the smooth surface of the fibers at the front (fig. 3.17). The fiber breaking is a result of back surface spallation which is a tensile failure. The fracture morphology is similar to that published by Dr. Silva¹⁸ where carbon fibers were stressed to failure in an extensometer.

In fig. 3.22 a cross section is shown for the above impact geometry. The cracks traverse the whole sample as fibers are not arresting crack propagation for those direction

3.6 Conclusion

A comparative study was presented for dynamic spall development in carbon epoxy unidirectional fiber composites, pure aluminum and iron. The very brittle fracture mode of the composites was observed at very low energy densities. However, the fracture was localized at the spall zone, and no internal delaminations or crack propagation were observed through the sample as an effect of shock wave propagation for impacts perpendicular to fiber direction.

When impacts were along the fiber direction, the cracks propagated through the sample because the fibers did not act as crack arresters. No crack branching was observed on the sectioned samples.

The intensive heat pulse ablated the matrix on the front, while tensile (spall) fracture without heating was evident at the back surface.

The unidirectional composite is stronger along the fiber direction than in the perpendicular direction. Quantitative comparison will be presented in the next section.

4. AN EXPERIMENTAL ESTIMATION OF THE LASER INDUCED SHOCK WAVE ATTENUATION IN DIFFERENT MATERIALS.

4.1 Introduction

High irradiance lasers can produce very strong shock waves in targets. The pressure pulse duration is comparable to the laser pulse length and consequently the shock attenuation is rapid. Diagnostics of high pressures in the range of kbars-Mbars on a nanosecond time scale is still a challenge, therefore calculations of these effects are achieved by large laser-matter hydrodynamic codes. These codes require a full understanding of many parameters and are therefore a major effort.

Analytic models have been developed^{21,22} for high irradiance lasers to calculate the formation and decay of laser generated shock waves. These models find that the pressure drops by more than a factor of two traversing a 50 μm aluminum slab for laser irradiances in the domain of $3 \cdot 10^{13} - 3 \cdot 10^{14}$ W/cm^2 .

Dynamic fracture and spall is a result of very short tensile stresses exceeding the dynamic strength of the material. Spall pressure is impact time dependent, however for very short transient times a reasonable prediction of dynamic spall strength (pressure) is needed. In our experiments, we have very short transient times and therefore the evaluation of the instantaneous dynamic spall strength is important.

A new approach is presented here to estimate experimentally the pressure gradient using the effect of spall in targets by laser induced shock waves. At threshold spall, we have the same spall pressure and the same shock velocity at the rear surface for different foil thicknesses. Using targets with decreasing thicknesses, the laser induced plasma ablation pressure P_{th} represents the real spall stress (P_s) and a value corresponding to pressure dispersion through the target thickness ΔX .

$$P_{th} = P_s + \frac{\partial P}{\partial X} \Delta X + \dots \quad (4.1)$$

By extrapolating the experimental values for zero thickness $\Delta X = 0$, the limiting value will represent the dynamic spall pressure. For small values of ΔX the Taylor expansion can be approximated by the first two terms given in eq. 4.1. In this case the slope will represent the pressure gradient. Experiments were performed to evaluate the pressure decay and spall pressure for isotropic and anisotropic materials using laser induced shock waves.

4.2 Experimental results

The experimental work consisted of determining the irradiance and energy density conditions required to produce spall in one dimensional shock wave geometry threshold conditions, see table 3.3.

The threshold pressure necessary to obtain incipient spallation of the samples was calculated from the plasma ablation pressure using the equation 1.1.

A linear dependence was obtained experimentally for the pressure as a function of target thickness for isotropic materials such as aluminum and iron. Similar experiments were performed on carbon fiber epoxy unidirectional composites for two impact geometries one for perpendicular

Impact vs fiber direction and the other along the fiber direction. see table 3.3 and fig. 4.1.

Our experiments yield directly the pressure gradient values. The values for P_{spall} were obtained by extrapolating to zero foil thickness (see table 4.1). In fig. 4.2 simulation results are presented for shock wave pressure attenuation in a 100 μm aluminum slab target for an irradiance of 10^{11} W/cm^2 . It is interesting to point out the ablation pressure calculated by eq. 1.1 for aluminum for a laser irradiance of 1×10^{11} W/cm^2 is the same as the value obtained from the simulation, which is 34 Kbar (see fig. 4.2).

The pressure gradient from fig. 4.2 (simulation) is 0.135 (Kb/ μm) while the experimental value for aluminum pressure gradient is 0.057 (Kb/ μm). This is about a factor of two less than the simulation values. The simulation results are less accurate for the lower pressure regions that prevail at the back free surface of the sample, because our simulation is a fluid code and therefore does not take into account material strength. It is therefore probable that our experimental results are more reliable than our simulation results in the domain of low pressure.

In table 4.2 a compilation (see references) of impact tensile strength for carbon and graphite epoxy unidirectional composites is made. We see that our method fit well with other published data. By analyzing the results for impact along fiber direction we see that for low strain rate (drop weight, instron) the tensile strength is higher than for higher strain rates (Hopkinson bar or explosive pressure pulse). Our experimental results correspond to the highest strain rate and therefore are consistent with the compilation of the experimental results, suggesting that P_{spall} decreases with increasing strain rate for composite materials. However, it might be possible that the different values of P_{spall} are due to specimen preparation.

V. DISCUSSION

A new experimental method was described to estimate the pressure gradient for laser induced shock waves in thin slab targets. The following values were obtained: aluminum has 57 ± 6 Kb/mm, iron has 154 ± 15 Kb/mm, for carbon fiber/epoxy composite it is 16 ± 2 Kb/mm when the impact is perpendicular to the fiber direction and 103 ± 10 Kb/mm when the impact is parallel (or along) the fiber direction. The large difference between the pressure gradient for perpendicular or parallel impact in unidirectional CF/epoxy is an experimental confirmation that the dispersion of the shock wave is significantly higher in the parallel direction. These results emphasize the tensor characteristics of anisotropic materials.

The dynamic spall pressure for very short impacts was obtained by extrapolating the threshold values for zero target thickness to eliminate the contribution of the pressure dispersion. The following values were obtained: aluminum 26 ± 2 Kbar, iron 57 ± 5 kbar, carbon/epoxy composite (perpendicular to fiber direction) is 0.3 ± 0.2 Kb and 7 ± 0.5 for impact parallel to the fiber direction.

The damage development in different carbon based composites was presented. Fracture morphologies emphasized the differences between front (ablation) or back (tensile) fracture modes. Densification of carbon-carbon composites by hot isostatic press provided a better penetration resistance material as compared to material densified at atmospheric pressure.

Acknowledgement

The research reported herein has been sponsored in part by the United States Army through its European Research Office. We are grateful for this support.

The authors would also like to acknowledge the scientific collaboration of Drs. S. Skholnik, H. Weissshaus and Y. Gazit and the devoted technical assistance of Mr. Y. Sapir, S. Maman and M. Gur.

REFERENCES

1. D. J. Boll, W.D. Bascom, J.C. Weidner, W.J. Murri, "A microscopy study of impact damage of epoxy-matrix carbon-fibre composites", *J. of Mat. Sci.* **21**, 2667 (1986).
2. J. Harding, L.M. Welsh, "A tensile testing technique for fibre-reinforced composites at impact rates of strain" *J. of Mat. Sci.* **18**, 1810 (1983).
3. T.R. Guess and E.D. Reedy, Jr., "Damage characterization and residual properties of shock-loaded S-2 Glass/epoxy laminates", SANDIA REPORT, SAND-86-1233C, (1986).
4. T.R. Guess, "Kevlar/epoxy laminates: Mechanical response of as fabricated and shock loaded materials", SANDIA REPORT, SAND-87-0620, (1987).
5. D.P. Fanucci, "Thermal response of radiantly heated kevlar and graphite epoxy composites", *J. of Composite Materials* **21**, 129 (1987).
6. D.R. Brighton, "The reflectance and thermal response of graphite fiber reinforced epoxy during irradiation by a high power CO₂ laser", Report No. MRL-R-1014, 1986, Department of Defence, Australia.
7. Loskarev, V.A., "Physics of the Destruction of and Problems of Heat Transfer in Carbon-Graphite Materials with Flow of Nitrogen Plasma." *Fizika Goreniya Vzryva*, **22**, 84 (1986).
8. Evangelides, J.S., "Laser Irradiation of Carbon Fibers and Composites," AD-A063783 (1979).
9. I. Gilath, D. Salzman, M. Givon, M.P. Dariel, L. Kornblith, T. Bar Noy, "Spallation as an effect of laser induced shock waves", *J. of Materials Science*, **23**, 1825 (1988).
10. I. Gilath, S. Eliezer, M.P. Dariel, L. Kornblit "Total elongation at fracture at ultra-high strain rates", *J. Mat. Sci. Letters*, **7**, 915 (1988).
11. I. Gilath, S. Eliezer, M.P. Dariel, L. Kornblit "Brittle to ductile transition in laser induced spall at ultra high strain rate", *Appl. Phys. Letters*, **52**, 1207 (1988).
12. D. Salzman, I. Gilath, B. Arad, "Experimental measurements of the conditions for the planarity of laser-driven shock waves", *Appl. Phys. Lett.*, **52**, 1128 (1988).
13. I. Gilath, S. Eliezer, M.P. Dariel, L. Kornblit, T. Bar Noy, "Laser induced spall in aluminum and copper", *J. de Physique C3*, **49**, 191 (1988).
14. M.H. Key "The physics of the superdense region" in Laser-Plasma Interactions edited by R.A. Cairns and J.J. Sanderson, Publ. SUSSP, p. 219, (1980).
15. D.E. Grady: "The spall strength of condensed matter", *J. Mech. Phys. Solids*, **36**, 353 (1988).
16. A.D. Krumbain, D. Salzman, H. Szichmann, S. Eliezer, Israel Atomic Energy Commission Report, IA-1396 (1985).
17. S. Jackel, M. Givon, a. Ludmirsky, S. Eliezer, J.L. Borowitz, B. Arad, A. Zigler, Y. Gazit: *Laser and Particle Beams* **5**, 115 (1987).
18. J.L.G. Da Silva and D.J. Johnson, "Flexural studies of carbon fibres," *J. of Mat. Sci.*, **12**, 3201 (1984).
19. Weisshaus, H.S. Kenig and E. Kastner, "Carbon/carbon Composites: Processing-Microstructure - Property Relationships," "Proceedings of the Denmark-Israel Binational Symposium on High Temperature Materials, Jerusalem (1986)

20. I. Gilath, S. Eliezer, H. Weissshaus, "Damage in 2D carbon/carbon composites by short pulsed laser induced shock waves", *J. of Reinforced Plastics and Composites*, 8, 259 (1989).
21. R.J. Trainor, Y.T. Lee: "Analytic models for design of laser generated shock-wave experiments". *Phys Fluids* 25, 1898 (1982)
22. A. Loeb and S. Eliezer "Analytical model for creation and decay of strong shock waves caused by a trapezoidal laser pulse". *Phys Fluids* 28, 1197 (1985)
23. P.N. Kousiounelos and J.H. Williams, "Dynamic fracture of unidirectional graphite fiber composite strips", *Int. J. of fracture* 20, 47 (1982).
24. I.M. Daniel, R.H. La Bedz and T. Liber, "New method for testing composites at very high strain rates", *Experimental mechanics*, 71 Febr (1981).
25. P.T. Curtis, "An investigation of the mechanical properties of improved carbon fibre composite materials" *J of Composite Mat.*, 21, 1118 (1987).
26. C. Cazeneuve and J.C. Maile "Etude du comportement des composites a fibres de carbon sous differente vitesses de deformation", *J de Physique*, 46, C5-551, (1985)
27. I. Gilath, S. Eliezer, S. Shkolnik, "Spall behaviour of carbon epoxy unidirectional composites as compared to aluminum and iron of composites", *J. of Composite Mat.* (to be published)

Table 2.1. C/C composites and their properties

Samples	Flexural Strength (kb) ASTM, D-790	Interlaminar Shear Strength (kb) ASTM, D-2344	Bulk Density (gr/cc)
0 + G)	0.48 ± 0.1	0.057	1.280
4(A + G)	0.68 ± 0.1	0.075	1.419
1(H + G)	1.20 ± 0.1	0.22	1.416

Table 2.2. Threshold irradiance for spallation of C/C composites for target thickness of 0.55 mm (for a laser pulse duration of 3.5 ns).

Sample	I_L Laser Irradiance Watt/cm ²	Laser Energy Density J/cm ²
0 + G	$(1.9 \pm 0.5) \times 10^{10}$	65 ± 20
4(A + G)	$(5.5 \pm 0.5) \times 10^{10}$	190 ± 30
1(H + G)	$(4.6 \pm 0.5) \times 10^{10}$	160 ± 30

Table 2.3. Perforation energy densities of C/C composites for target thickness of 0.55 mm.

Sample	Laser Energy Density (J/cm ²)
0 + G	1450 ± 300
4(A + G)	5950 ± 300
1(H + G)	>8650

Table 3.1. Typical properties of carbon fibers, aluminum and iron.

	CF	aluminum	iron	CF/epoxy
Tensile strength (static) [kbar]	33	0.5	1.8	12.4
Tensile modulus [kbar]	2300	620	1965	1350
Density [gr/cc]	1.78	2.7	7.8	1.47
Ultimate elongation (%)	1.55	60	18	-
Melting point (°C)	3550	660	1535	-

Table 3.2 Charpy method impact tests (ASTM-D256)

Sample	Impact strength Joule/cm	Impact pressure (calculated) kbar
CF/epoxy	11.6	0.18
Aluminum	28.1	0.44
Iron	41.7	0.65

Table 3.3 Threshold energy for spall, irradiance and plasma ablation pressure for carbon/epoxy unidirectional composite, aluminum and iron.

Sample thickness	Laser energy threshold for spall [J/cm ²]	Laser irradiance threshold for spall [Watt/cm ²]	Corresponding plasma ablation pressure, [kbar]
Aluminum			
0.100	280	8×10^{10}	28.7
0.175	350	1×10^{11}	33.9
0.275	460	1.3×10^{11}	41.4
0.600	700	2×10^{11}	57.2
Iron			
0.100	1060	3×10^{11}	69.4
0.250	1420	4×10^{11}	92.5
Carbon Epoxy Composite (perpendicular impact)			
0.2	25	3.3×10^9	2.2
0.5	195	2.6×10^{10}	8.6
0.9	325	4.3×10^{10}	13.8
2.0	650	8.6×10^{10}	25.2
Carbon Epoxy Composite (parallel impact)			
0.2	225	6.4×10^{10}	24.9
0.4	460	1.3×10^{11}	43.0
0.6	700	2.0×10^{11}	60.0
0.8	1150	3.4×10^{11}	86.8

Table 4.1. The spall pressure and pressure gradient in different materials.

Material	Pspall (kb)	Pgradient (kb/mm)
Iron	57 ± 5	154 ± 15
Aluminum	26 ± 2	57 ± 6
CF/Epoxy (perpendicular to fiber)	0.3 ± 0.2	16 ± 2
CF/epoxy (parallel to fiber)	7 ± 0.5	103 ± 10

Table 4.2 Dynamic tensile strength of unidirectional carbon or graphite epoxy composites (Impact configuration 0° is along fiber direction while 90° is perpendicular direction).

Material	Impact Configuration	Dynamic Method	Tensile Strength kb	Ref.
Graphite-epoxy	0°	Instron	17.2	23
	90°		0.4	
Graphite-epoxy	0°	Explosive pressure pulse in ring specimen	10-12	24
	90°		1.2-1.6	
Carbon epoxy	0°	Drop weight	17	25
	90°		1	
Carbon epoxy	0°	Hopkinson bar	12	2
Carbon epoxy	0°	Hopkinson bar	11.5	26
	90°		3.4	
Carbon epoxy	0°	Laser induced shock waves	7 ± 0.5	Our results
	90°		0.3 ± 0.2	

FIGURE CAPTIONS

- Fig. 1.1 Spall caused by a triangular pressure pulse. P_s = Spall pressure, P_0 = maximum pressure at the back surface, Δ = spall layer.
- Fig. 1.2 The laser system.
- Fig. 1.3 Partial view of the amplifier stage.
- Fig. 1.4 Target chamber.
- Fig. 2.1 Sample 4(A + G), spallation at 470 J/cm^2 , 3.5 nsec laser pulse.
- Fig. 2.2 Sample 4(A + G), spallation at 800 J/cm^2 , 3.5 nsec laser pulse.
- Fig. 2.3 Sample 4(A + G), spallation at 2360 J/cm^2 , 3.5 nsec laser pulse.
- Fig. 2.4 Sample 4(A + G), spallation at 4720 J/cm^2 , 3.5 nsec laser pulse.
- Fig. 2.5 Sample 4(A + G), back surface perforation at 5970 J/cm^2 , 3.5 nsec laser pulse, target thickness of 0.55 mm.
- Fig. 2.6 Sample 4(A + G), front surface perforation at 5970 J/cm^2 , 3.5 nsec laser pulse.
- Fig. 2.7 Glassy carbon in 1(H + G) sample, $1.2 \times 10^{12} \text{ W/cm}^2$, 9260 J/cm^2 .
- Fig. 2.8 Front surface damage for 1(H + G), 2800 J/cm^2 .
- Fig. 2.9 Detail from Fig. 2.8 showing fiber resolidification.
- Fig. 2.10 Detail from Fig. 2.8 showing matrix damage.
- Fig. 3.1 Irradiated threshold energy density for spall for different materials as a function of sample thickness (7.5 nsec laser pulse)
- Fig. 3.2 Front surface damage at 1470 J/cm^2 , for carbon epoxy composite, impact perpendicular to fiber direction
- Fig. 3.3 Detail from figure 3.2
- Fig. 3.4 Front surface damage in aluminum, 2.2 KJ/cm^2
- Fig. 3.5 Incipient damage on back surface at 195 J/cm^2 , for carbon epoxy composite, impact perpendicular to fiber direction.
- Fig. 3.6 Fracture development at back surface at 515 J/cm^2 , for carbon epoxy composite, impact perpendicular to fiber direction.
- Fig. 3.7 Fracture development at back surface at 740 J/cm^2 , for carbon epoxy composite, impact perpendicular to fiber direction.
- Fig. 3.8 Detail from figure 3.7
- Fig. 3.9 Back surface damage at 6000 J/cm^2 , for carbon epoxy composite, impact perpendicular to fiber direction (40x).
- Fig. 3.10 Cross section of a 2 mm sample, at 650 J/cm^2 , for carbon epoxy composite, impact perpendicular to fiber direction, (23x).
- Fig. 3.11 Incipient spall in aluminum at 1.55 KJ/cm^2 , (200x).
- Fig. 3.12 Incipient spall in iron at 2.4 KJ/cm^2 (140x).
- Fig. 3.13 Undamaged material for carbon epoxy composite (section perpendicular to fiber direction).
- Fig. 3.14 Front surface for carbon epoxy composite after laser impact at 1320 J/cm^2 , 3.5 nsec laser pulse.
- Fig. 3.15 Front surface damage for carbon composite (parallel to fiber direction impact), 1320 J/cm^2 , 3.5 nsec laser pulse.
- Fig. 3.16 Irregular cracking of front surface, for carbon epoxy composite 530 J/cm^2 , 3.5 nsec laser pulse.
- Fig. 3.17 Detail from front surface damage, for carbon epoxy composite ablated matrix revealing smooth carbon fibers (60° tilt), 1320 J/cm^2 , 3.5 nsec laser pulse
- Fig. 3.18 Front surface of carbon epoxy near the impact site with partially debonded matrix, 1320 J/cm^2 , 3.5 nsec laser pulse.
- Fig. 3.19 Back surface cracking of carbon epoxy, 1320 J/cm^2 , 3.5 nsec laser pulse.
- Fig. 3.20 Fiber and matrix breaking at the back surface, of carbon epoxy 1320 J/cm^2 , 3.5 nsec laser pulse.
- Fig. 3.21 Typical fiber breaking of carbon epoxy, 1320 J/cm^2 , 3.5 nsec laser pulse.

- Fig. 3.22. Cross section through impact along the fiber distance, for carbon epoxy composition, 1320 J/cm^2 , 3.5 nsec laser pulse.
- Fig. 4.1. Threshold plasma ablation pressure for spall as a function of target thickness.
- Fig. 4.2. Simulation of shock wave decay in an $100 \text{ }\mu\text{m}$ aluminum target for $I = 10^{11} \text{ W/cm}^2$.

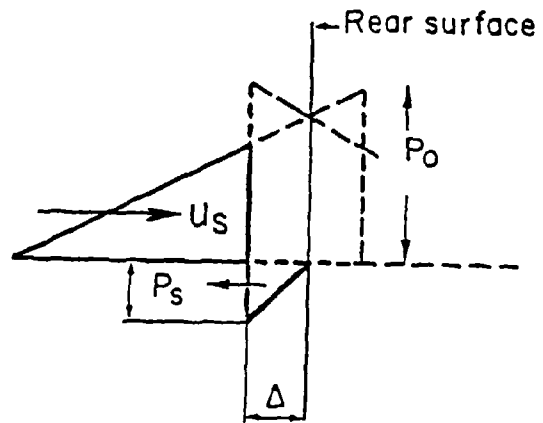


Fig. 1.1

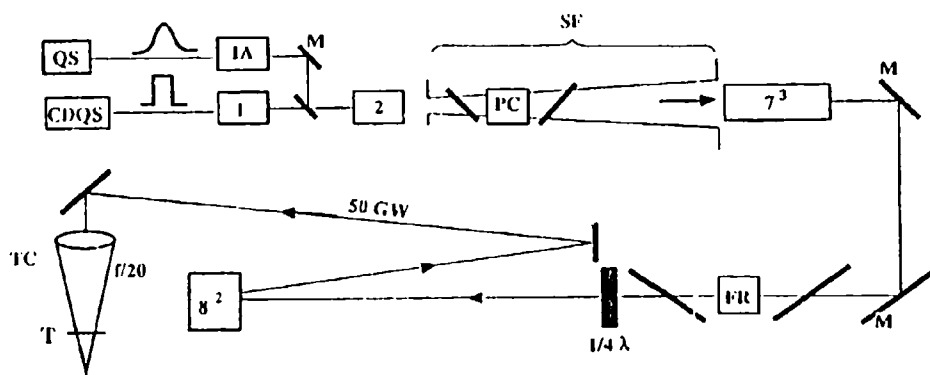


Fig. 1.2



Fig. 1.3



Fig. 1.4

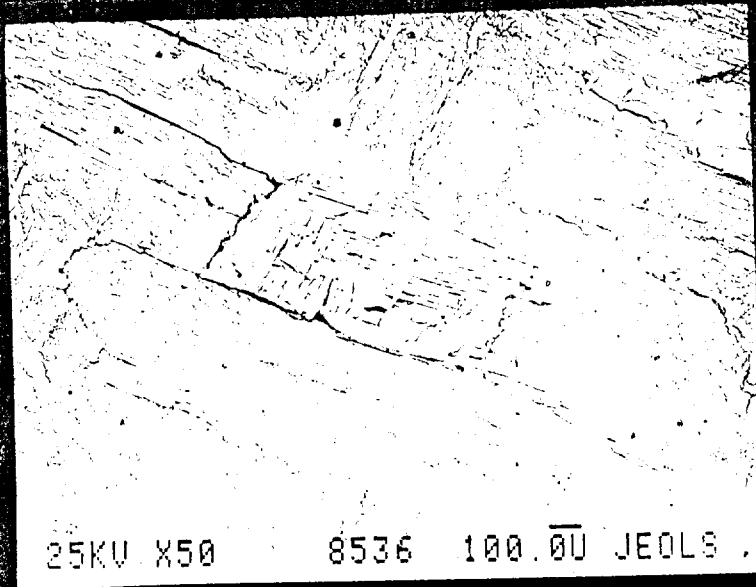


Fig. 2.1

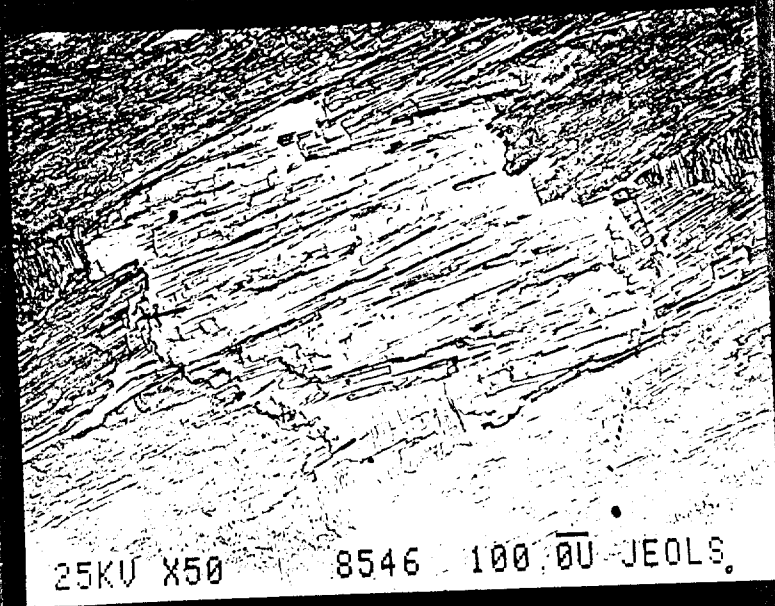


Fig. 2.2

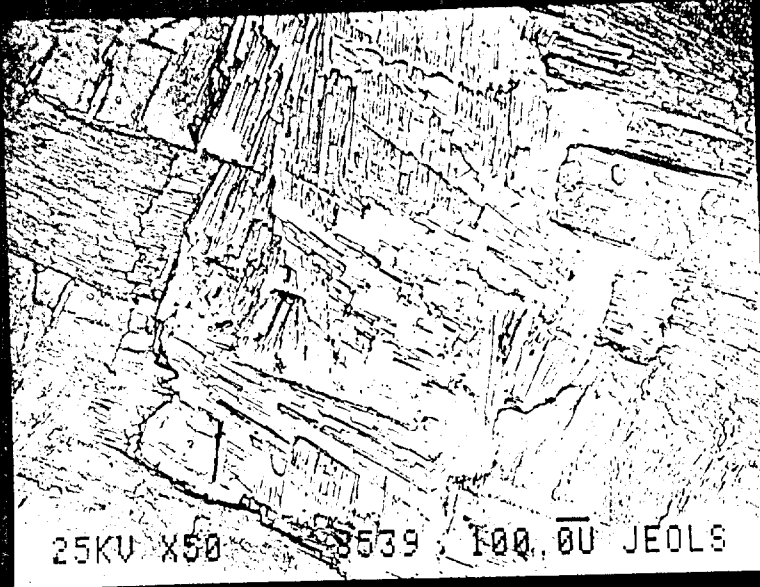


Fig. 2.3

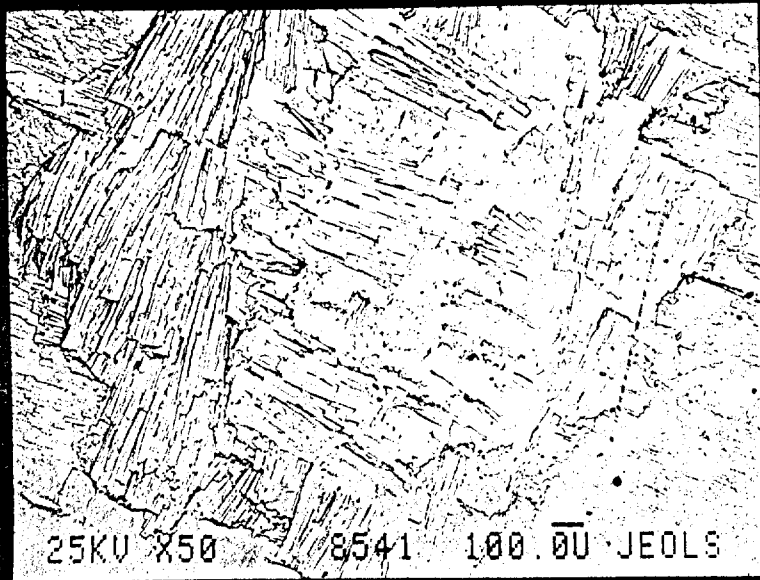


Fig. 2.4

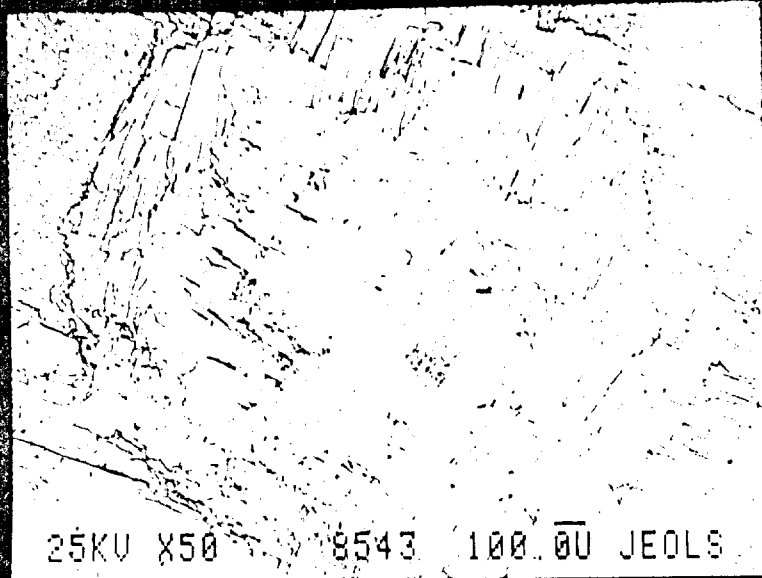


Fig. 2.5

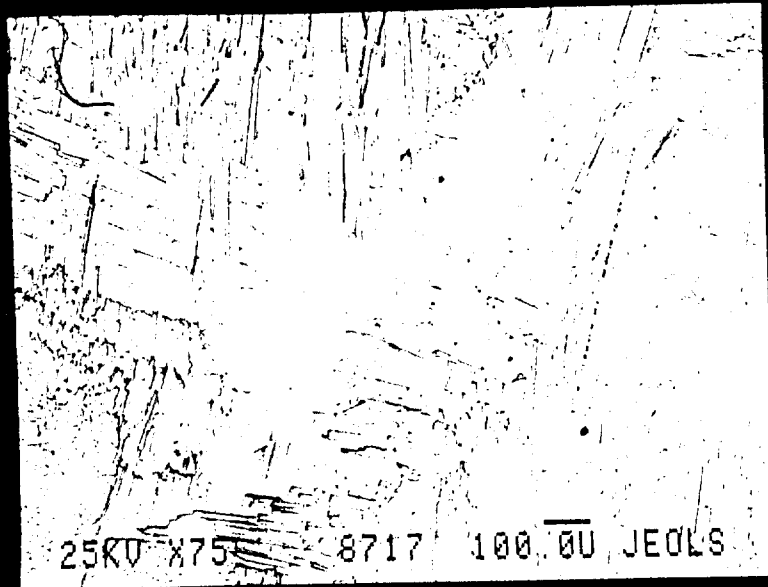


Fig. 2.6

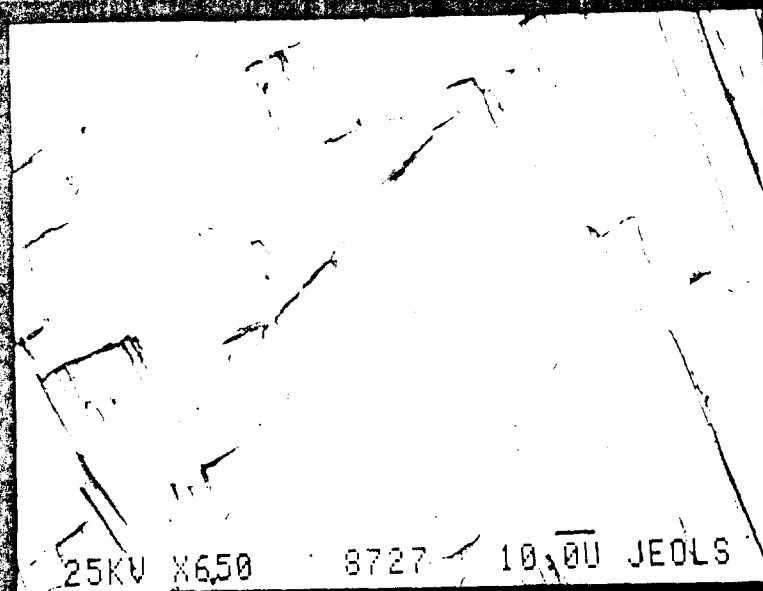


Fig. 2.7

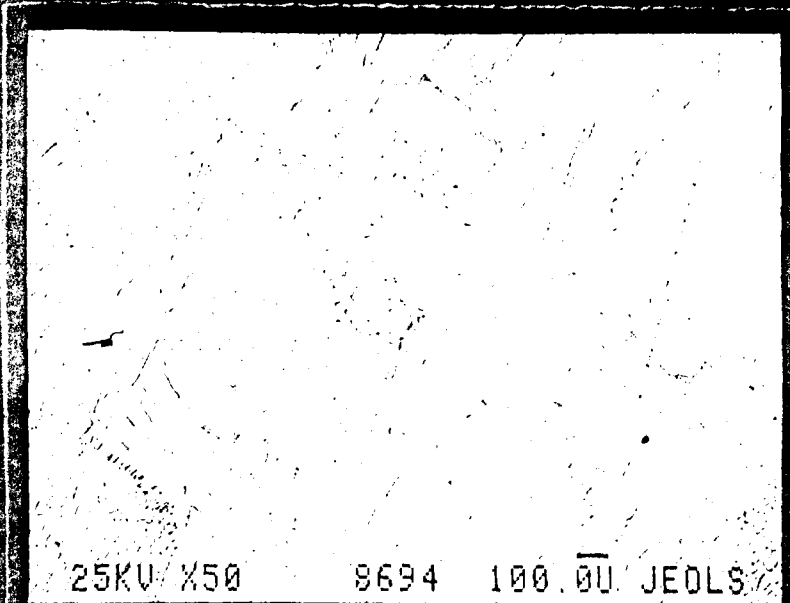


Fig. 2.8

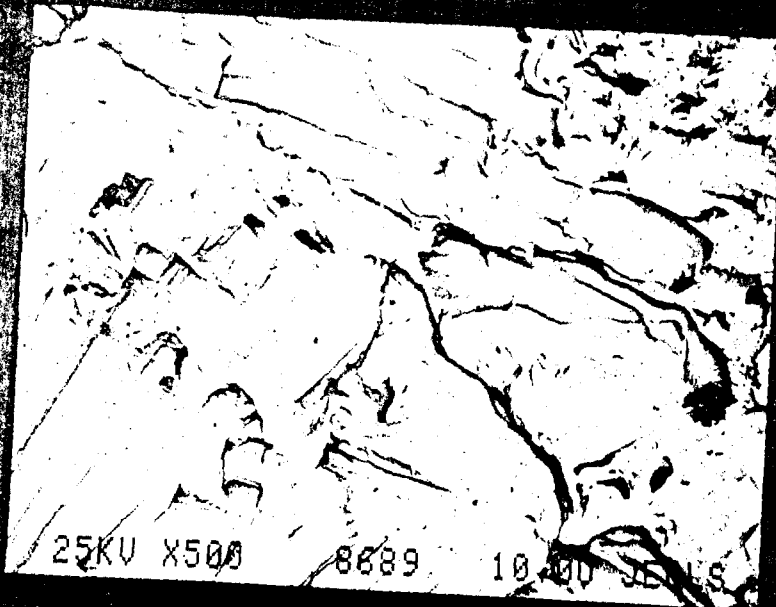


Fig. 2.9

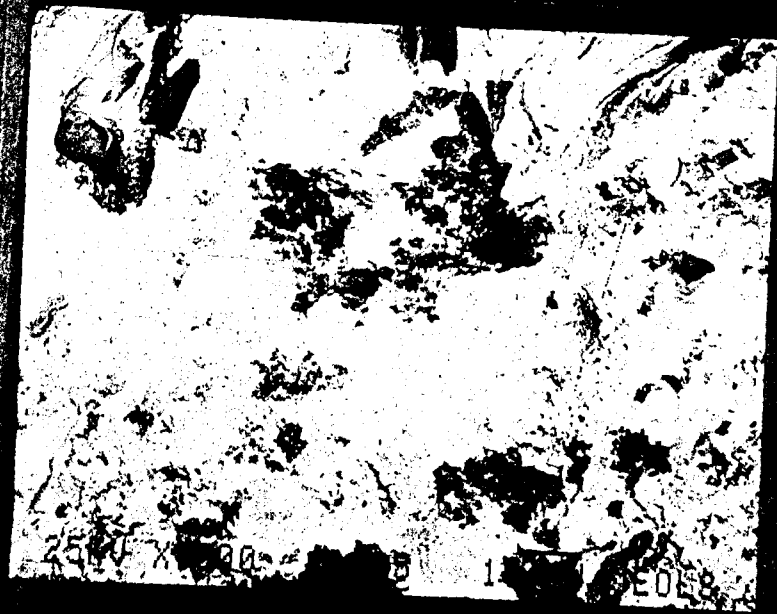


Fig. 2.10

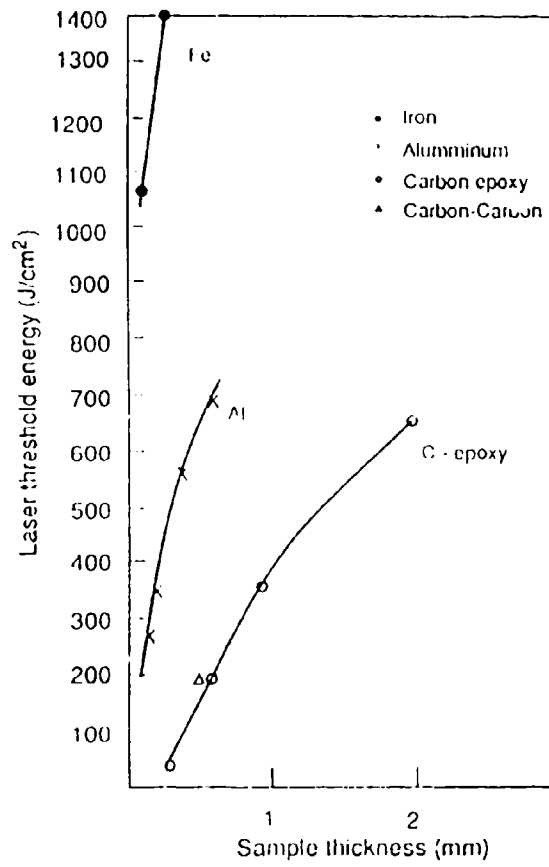


Fig. 3.1

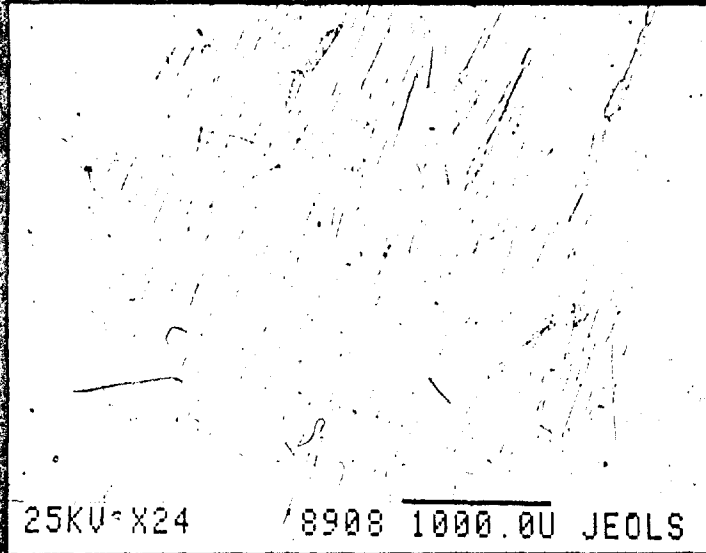


Fig. 3.2

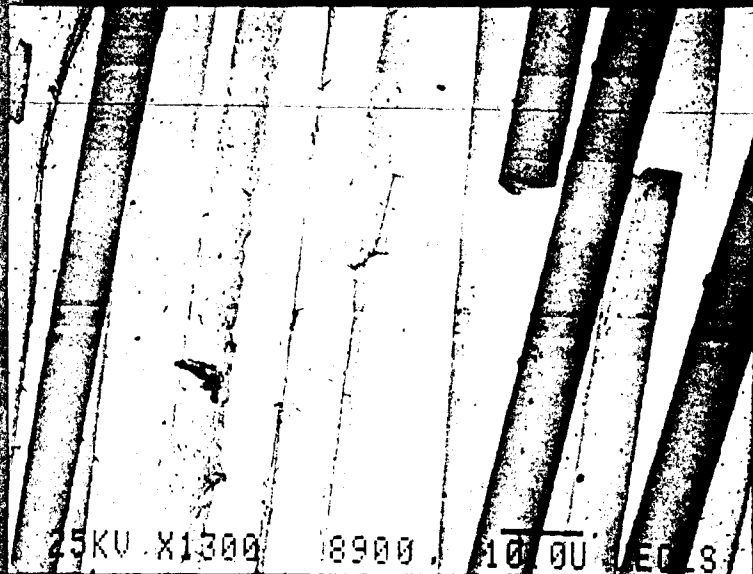


Fig. 3.3



Fig. 3.4

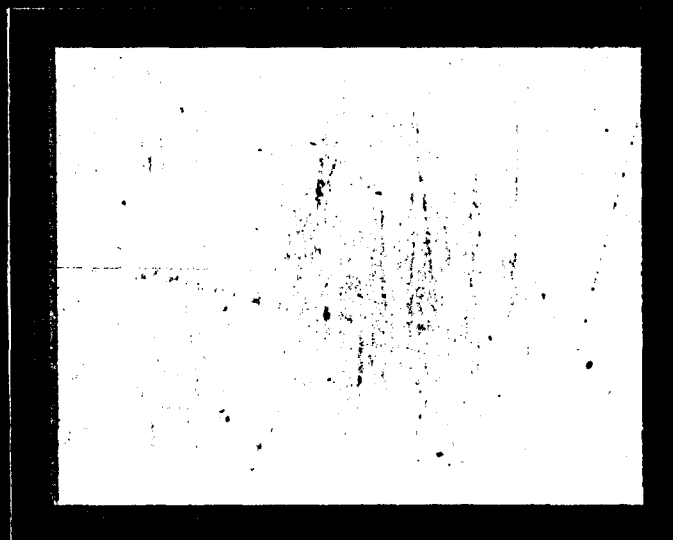


Fig. 3.5

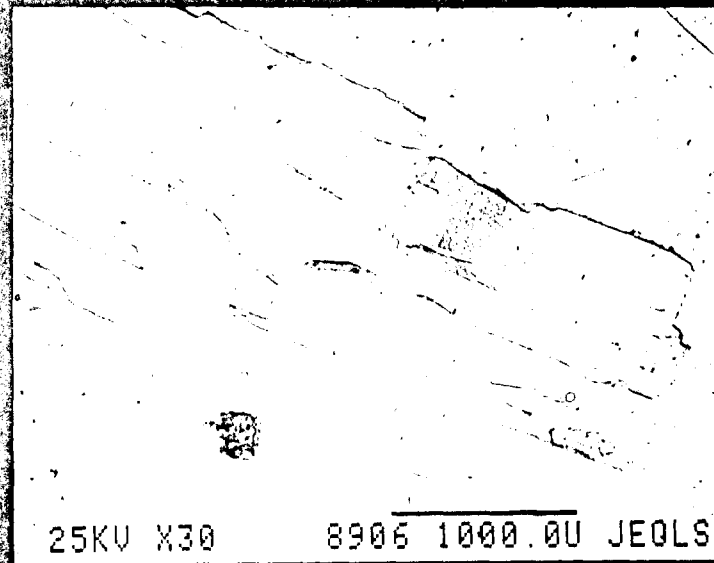


Fig. 3.6

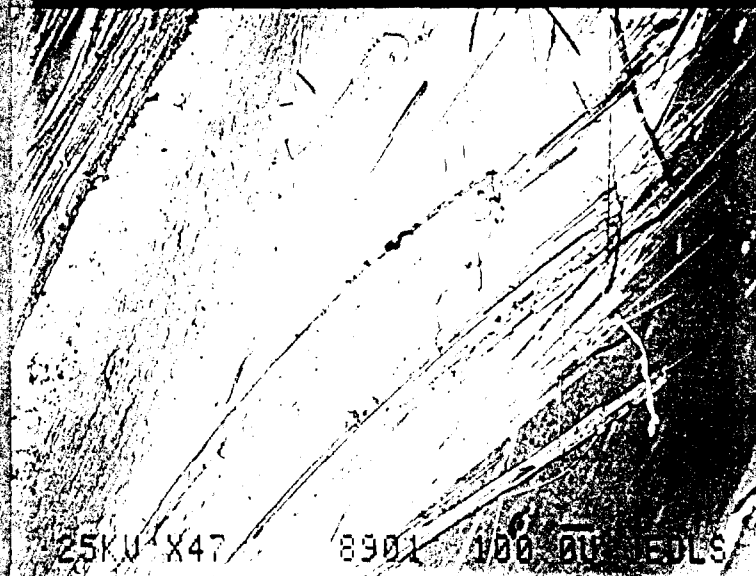


Fig. 3.7

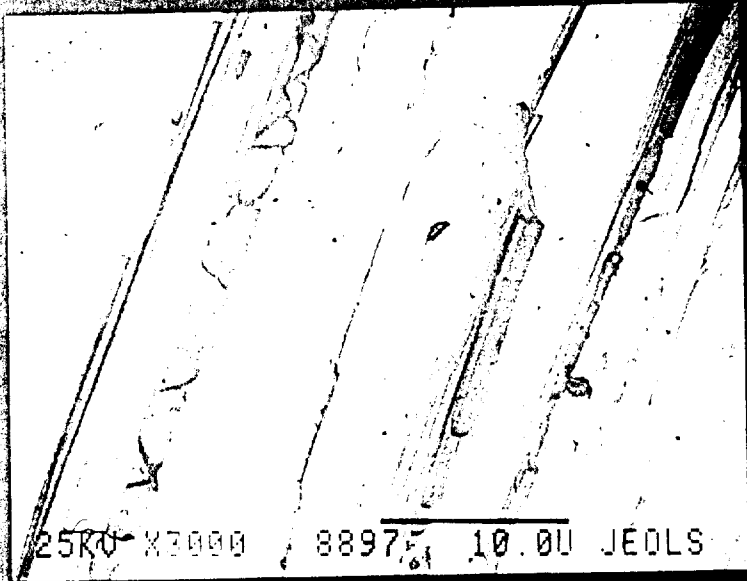


Fig. 3.8



Fig. 3.9



Fig. 3.10

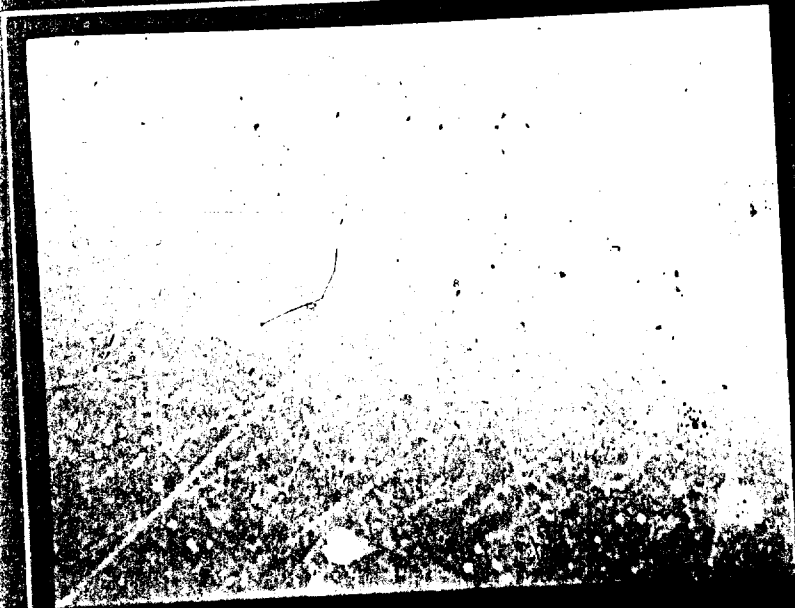


Fig. 3.11

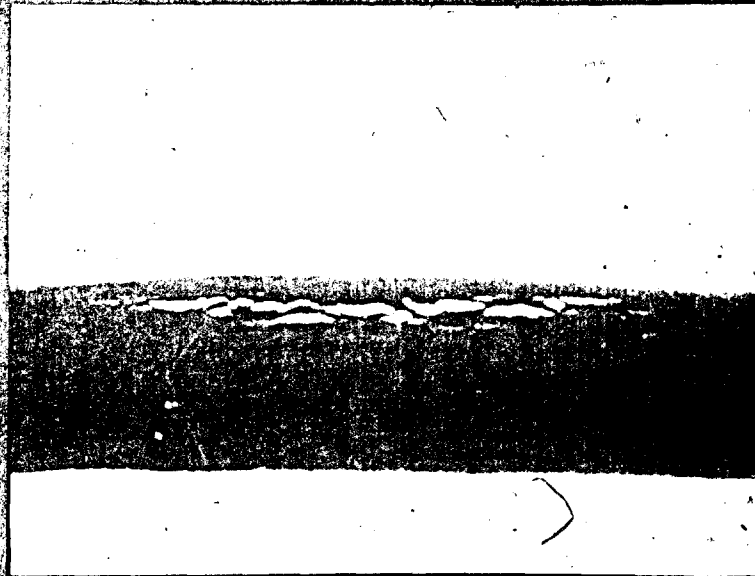


Fig. 3.12

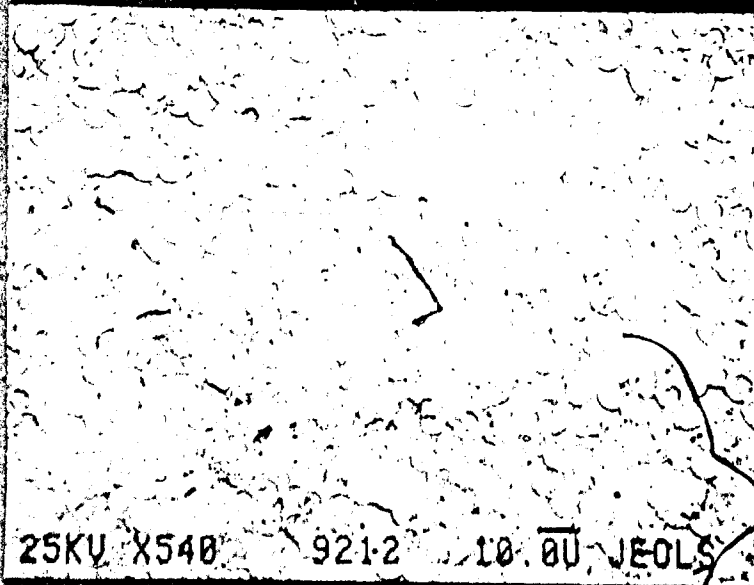


Fig. 3.13

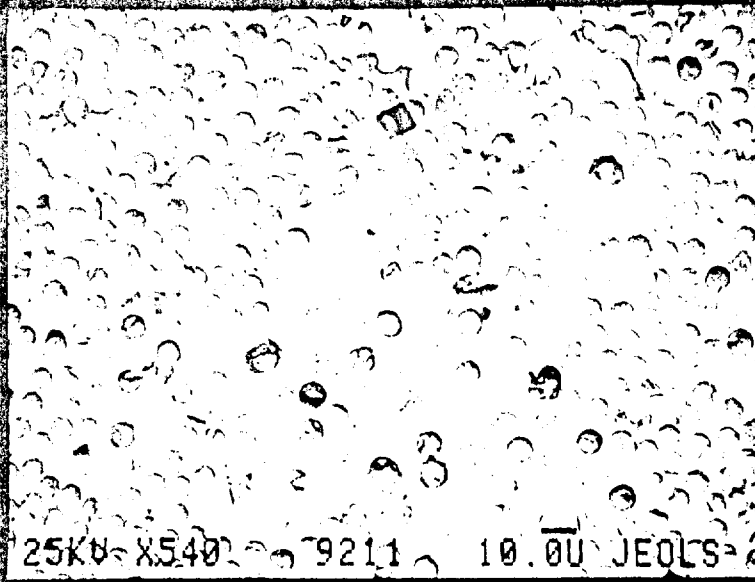


Fig. 3.14

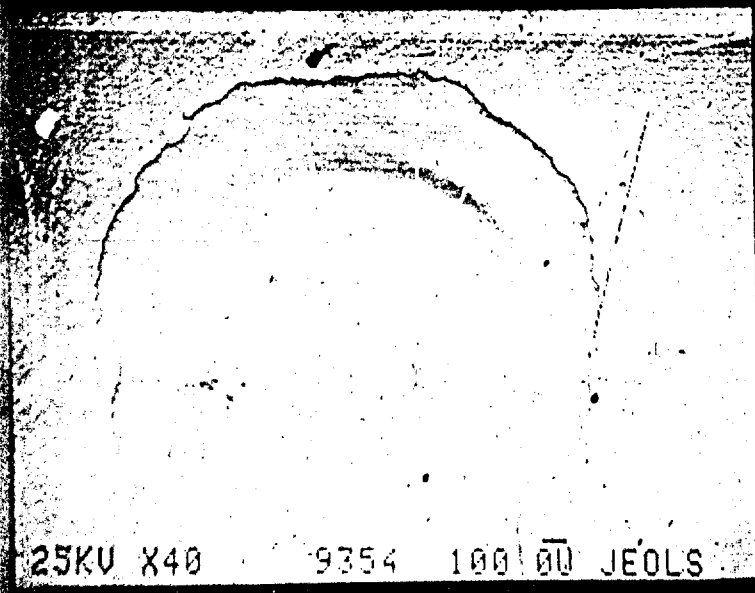


Fig. 3.15

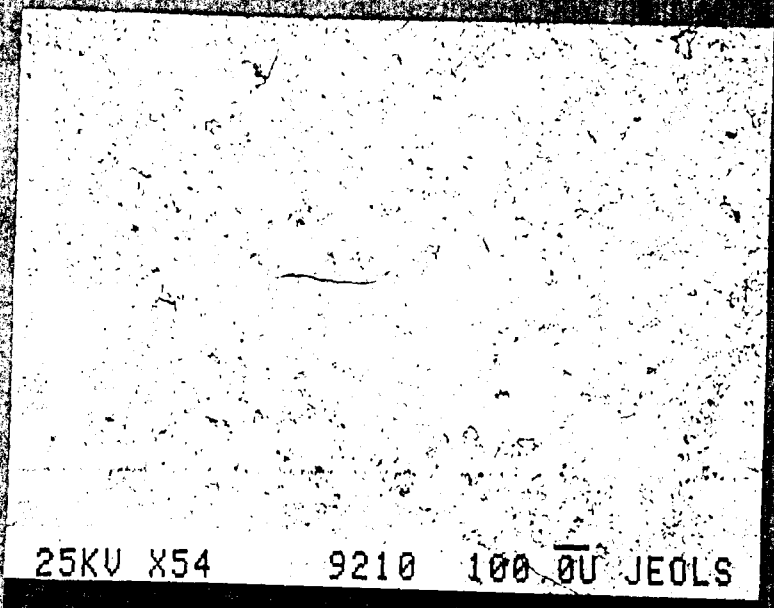


Fig. 3.16

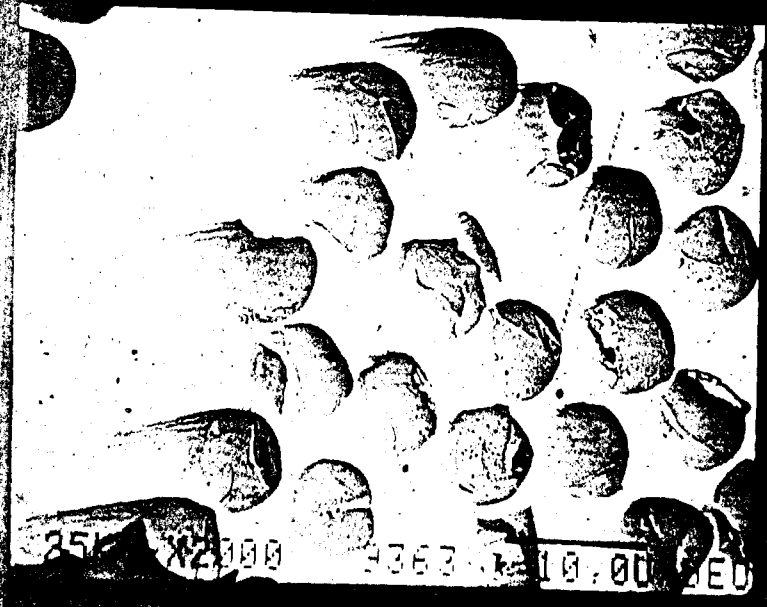


Fig. 3.17

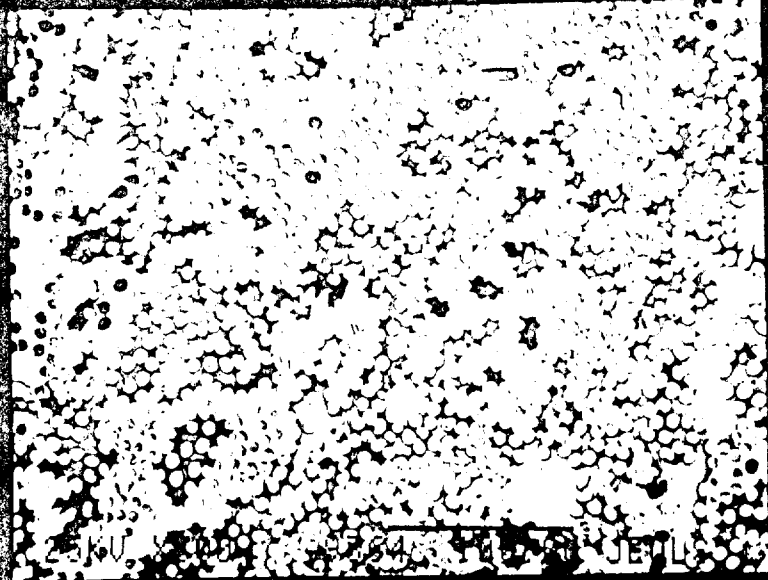


Fig. 3.18

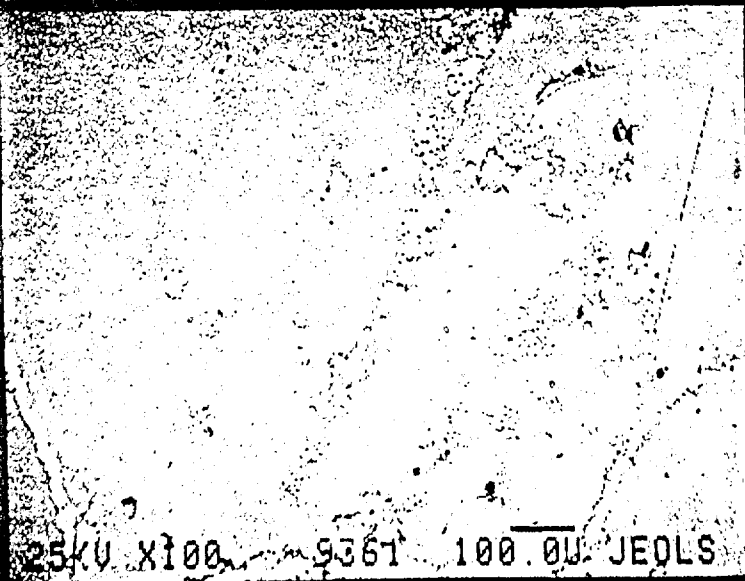


Fig. 3.19

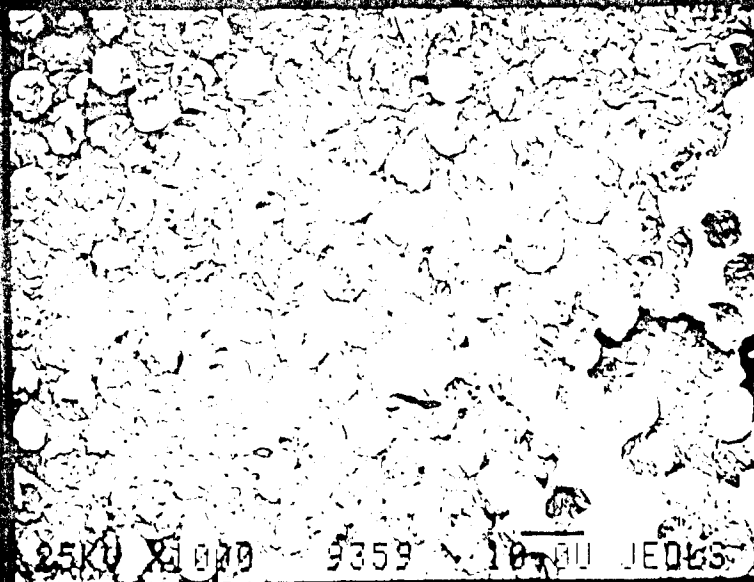


Fig. 3.20

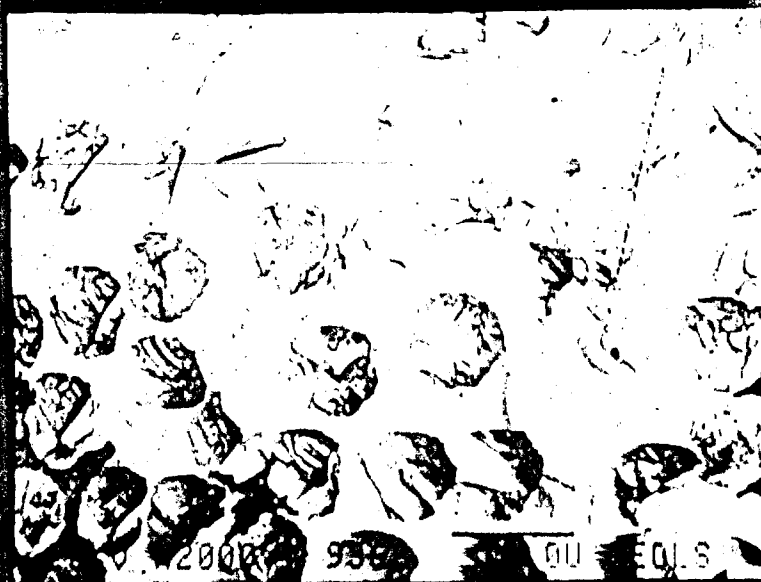


Fig. 3.21

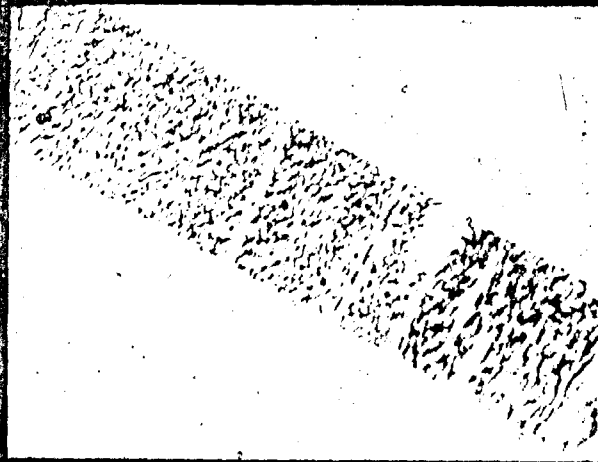


Fig. 3.22

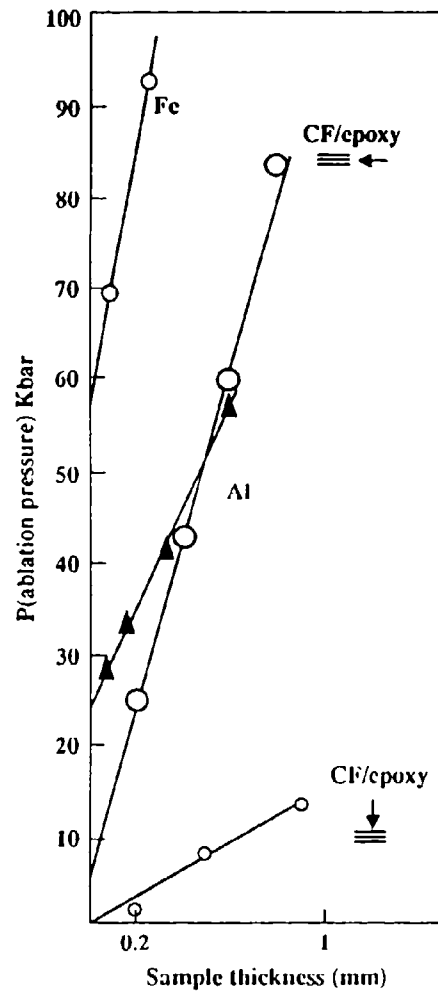


Fig. 4.1

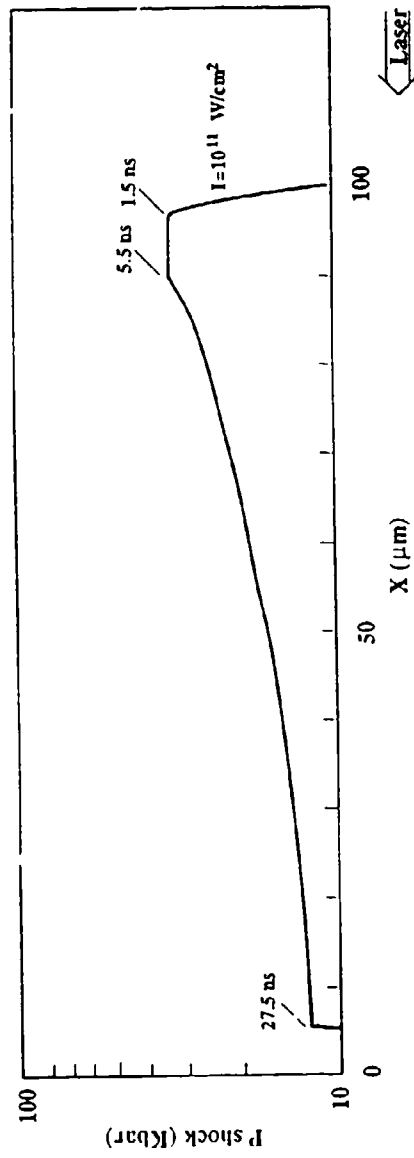


Fig. 4.2